Supplemental Figure 1

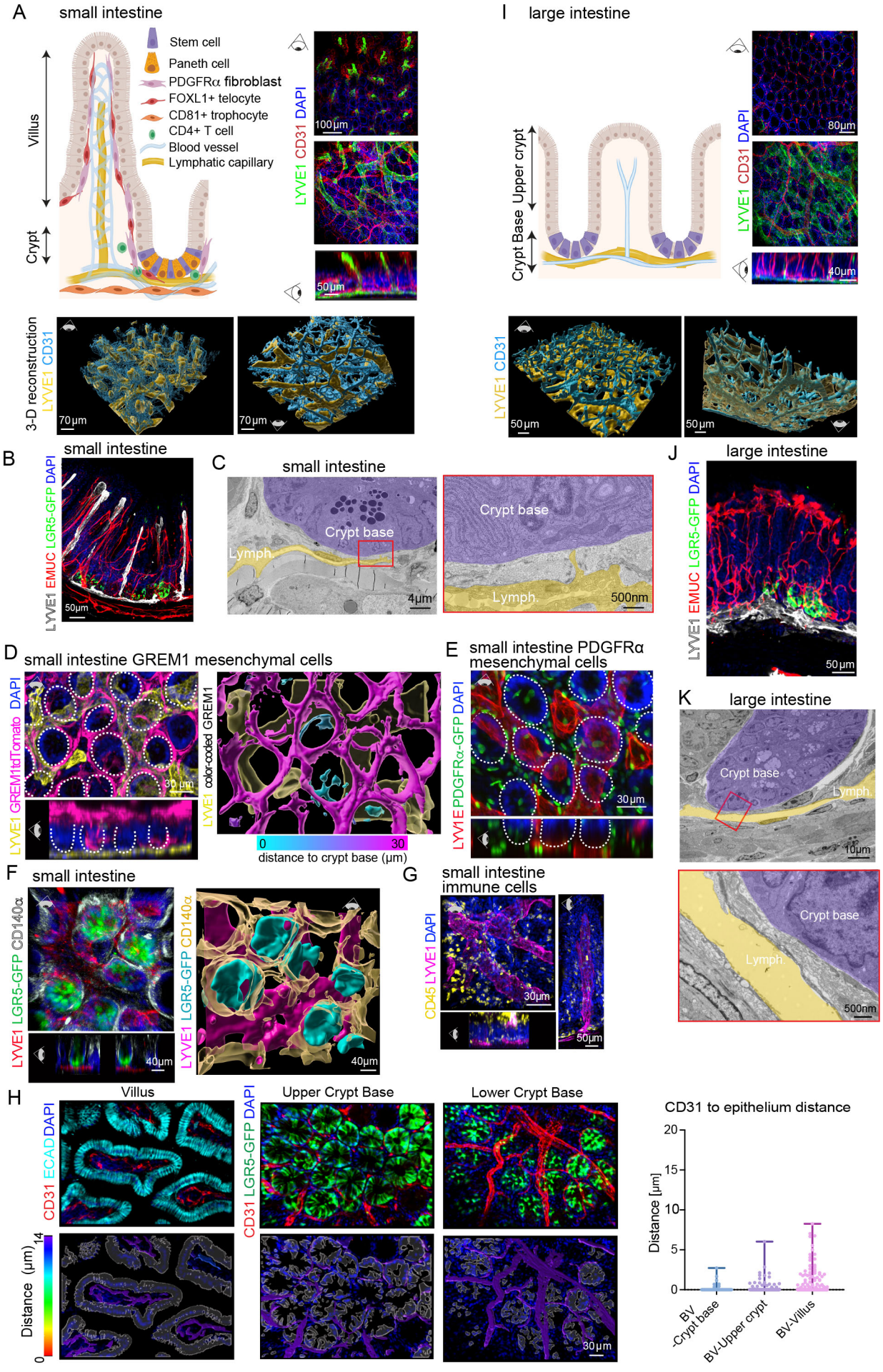

Figure S1. **Lymphatics integrate with neighboring intestinal stem cell niche cells to access the crypt base, Related to Figure 1. (A)** Left: schematic of the small intestinal crypt niche, indicating cell types approximating the crypt base and their integration with the lymphatic niche. Right: 3D images of the small intestinal vasculature in the villus illustrating LYVE1$^+$ lymphatics (green) and CD31$^+$ blood endothelial cells (red). Bottom two panels: representative 3D-volumetric reconstruction of vascular structures including lymphatics (LYVE1$^+$, yellow) and blood vessels (CD31$^+$, blue). **(B)** 3D image of the lymphatic vasculature (LYVE1$^+$, white), blood vessels (EMUC$^+$, red) and crypt-based LGR5$^+$ stem cells (green) in the small intestine of Lgr5-EGFP-IRES-CreERT2 mice. **(C)** EM image demonstrating the crypt base (purple, identified by granules within Paneth cells) and lymphatic capillaries (yellow). The inset (red box) demonstrates a lymphatic endothelial cell projection towards the crypt base. **(D)** 3D images of GREM1$^+$ stromal cells, lymphatics (LYVE1$^+$) and crypts (DAPI$^+$, outlined by dotted lines) in Grem1-CreERT2-tdTomato$^{flox/flox}$ mice. The left panel shows the original immunofluorescent image, while the right panel shows 3D-reconstructed GREM1$^+$ stromal cells color-coded by their distance to the crypt base. **(E)** 3D image of small intestinal crypts demonstrating the relationship between PDGFRα-GFP$^+$ stromal cells, the lymphatic vasculature (LYVE1$^+$) and DAPI$^+$ crypts (white dotted outline) in PDGFRα-H2B-eGFP mice. **(F)** 3D image of small intestinal tissue stained for PDGFRα/CD140a, LYVE1, and LGR5-GFP in Lgr5-eGFP-IRES-CreERT2 mice demonstrating the relationship between PDGFRα^+ mesenchymal niche cells, lymphatics and crypt-based stem cells. 3D reconstruction is in the right side panel. **(G)** 3D images of mouse small intestinal tissue demonstrating the spatial relationship between CD45$^+$ immune cells, LYVE1$^+$ lymphatics and epithelial cells (DAPI$^+$) of intestinal crypts and villi with the left panel illustrating the crypt region and the right panel illustrating the full crypt-villus axis and a lymphatic lacteal. **(H)** 3D images of 5 µm z-stacks of the mouse small intestinal blood vasculature and intestinal epithelial cells (ECAD+, villus) or intestinal epithelial stem cells (LGR5-GFP+, upper and lower crypt base). Quantification of the distance between vascular surfaces and the epithelium was done as for lymphatics in figure 1E (n= 9 mice with 3 images/region/mouse). No significant difference (one-way ANOVA with Tukey's multiple comparisons) was observed. **(I)** 3D images of the large intestinal vasculature (LYVE1+ lymphatics, CD31+ endothelial cells)

in the upper crypt and crypt base with a schematic on the left. Bottom panels show representative 3D volumetric reconstruction images of vascular structures. **(J)** 3D image of the lymphatic vasculature (LYVE1$^+$, white), blood vessels (EMUC$^+$, red) and crypt-based LGR5$^+$ stem cells (green) in the large intestine of Lgr5-EGFP-IRES-CreERT2 mice. **(K)** EM image demonstrating the crypt base (purple) and lymphatic capillaries (yellow). The inset (red box) demonstrates a lymphatic capillary in proximity to the crypt base. All images are representative of *n* = 3 or more mice/group with 3 or more images/mouse/region imaged.

Supplemental Figure 2

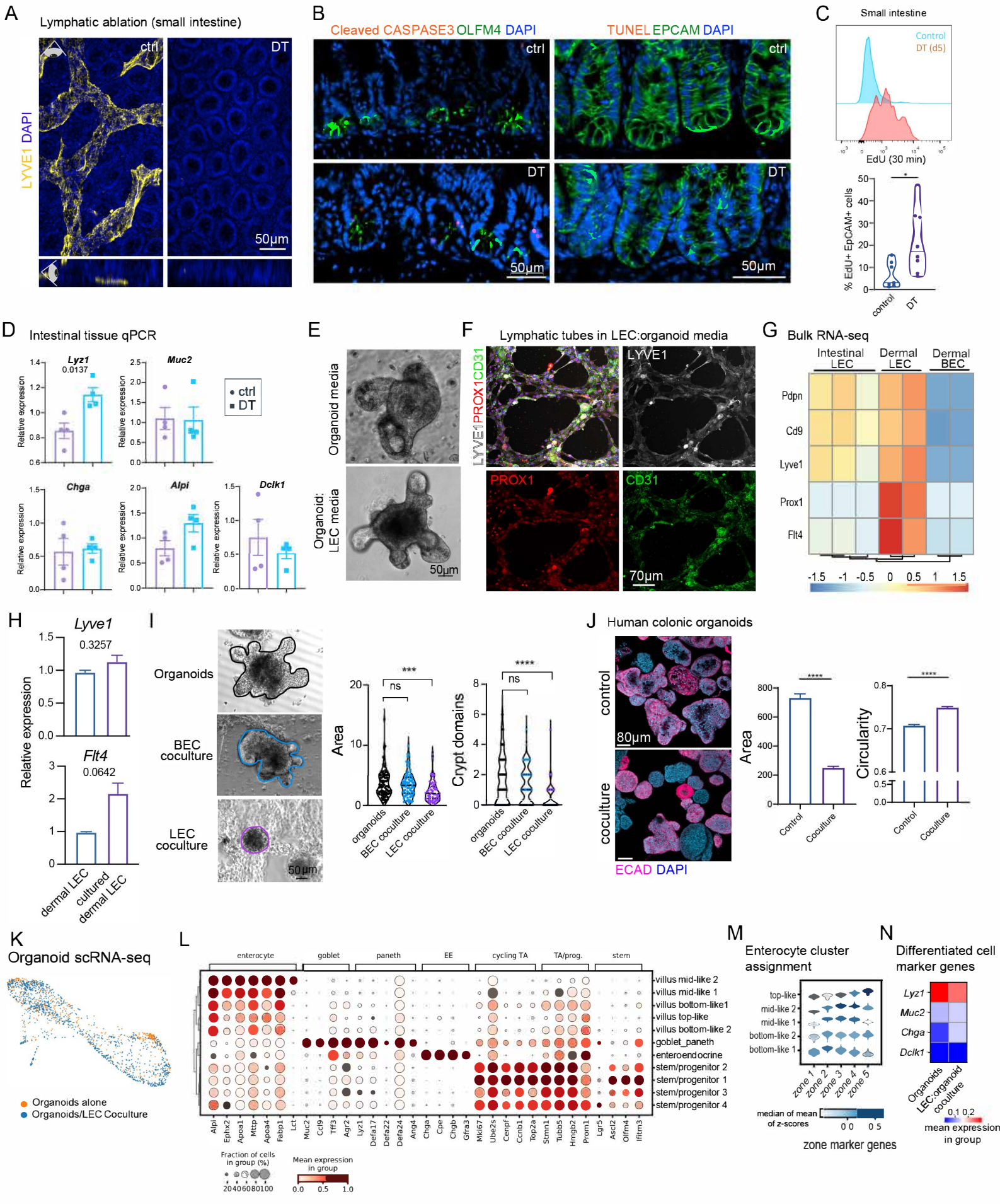

Figure S2. **Lymphatics support intestinal stem cell maintenance and decrease enterocyte differentiation, Related to Figure 2 and Figure 3. (A)** Lymphatic ablation (LYVE1+ lymphatic capillaries) in the small intestine of *Vegfr3-CreERT2 iDTR*$^{fl/+}$ mice treated with PBS (control) and DT as per schematic in figure 2A. **(B)** Representative images of Cleaved CASPASE3 (left) and TUNEL (right) in control and DT-treated mice (*n* =3 independent experiments with 3 or more mice per group). **(C)** Histogram and quantification of EdU+ cells after a 30-minute-pulse in control and DT-treated mice analyzed by flow cytometry, corresponding to figure 2D (top). **(D)** Quantitative real-time PCR of intestinal epithelial differentiation markers: The expression of *Lyz1* (Paneth cells), *Muc2* (goblet cells), *Chga* (enteroendocrine cells), *Alpi* (mature, differentiated enterocytes), *Dclk1* (tuft cells) is shown in control vs DT-treated *Vegfr3-CreERT2 iDTR*$^{fl/+}$ mice (*n* = 3 experiments) **(E)** Representative brightfield images of small intestinal organoids cultured in 100% organoid medium (top) and 50%:50% LEC:organoid medium (bottom). **(F)** Representative immunofluorescence images of cultured LECs at passage 5. LECs maintain common endothelial markers such as CD31 (green) and lymphatic-specific markers LYVE1 (white) and PROX1 (red) while grown in 50:50 co-culture media. **(G)** Z-scored expression values of lymphatic and blood vasculature genes from bulk RNA-sequencing of intestinal lymphatics and dermal lymphatics and blood vasculature (Gur-Cohen et al., 2019). Each column is an individual mouse. **(H)** Quantitative real-time PCR of lymphatic markers *Lyve1* and *Flt4/Vegfr3* in cultured versus *ex vivo* isolated dermal lymphatic endothelial cells (LECs). **(I)** Left: Representative images of small intestinal organoids cultured alone or cocultured with LECs and blood endothelial cells (BECs). Tracing of organoid shape was done in ImageJ for subsequent quantification of morphological parameters (area) on the right. Right: Violin plots of the area and number of crypt domains per organoid of small intestinal organoids cultured alone, cocultured with BECs or LECs (*n* = 3 independent experiments). **(J)** Left: Representative images of human colonic organoids cultured in the presence or absence of human LECs on day 4 of culture. Right: Quantification of the size (area) and circularity per organoid (representative of *n* = 2 experiments utilizing organoids from *n* = 5 biological replicates. Approximately 2000 organoids were quantified per condition). **(K)** Force-directed layout of scRNA-seq data of small intestinal organoids that were cultured in the absence (orange

dots) and presence (blue dots) of LECs. **(L)** Dot plot of marker genes used for cell type-specific cluster assignment of sequenced epithelial cells from organoids cultured in the presence or absence of LECs. The size of the dots represents the fraction of cells with non-zero expression in each group, while the color indicates log-transformed library size-normalized gene expression values. Genes are indicated at the bottom, and the cell types that each gene represents was shown at the top. PhenoGraph clusters are indicated on the right. EE = enteroendocrine cell, cycling TA. = cycling transit-amplifying (TA) cell, TA/prog. = TA/progenitor cell. **(M)** Violin plot shows the log-transformed library size-normalized gene expression values of villus enterocyte zone signatures (Moor *et al*., 2018) (x-axis) in each PhenoGraph cluster of enterocytes (y-axis). **(N)** Expression of Lysozyme (*Lyz1*, Paneth cells), Mucin2 (*Muc2*, goblet cells), Chromogranin A (*Chga*, enteroendocrine cells) and *Dclk1* (tuft cells) in organoids alone versus cocultured organoids. For all experiments with asterisk, * p-value 0.01 to 0.05, ** p-value of 0.001 to 0.01, *** p-value of 0.0001 to 0.001, **** $p < 0.0001$ (Unpaired two-tailed Student's *t*-test).

Supplemental Figure 3

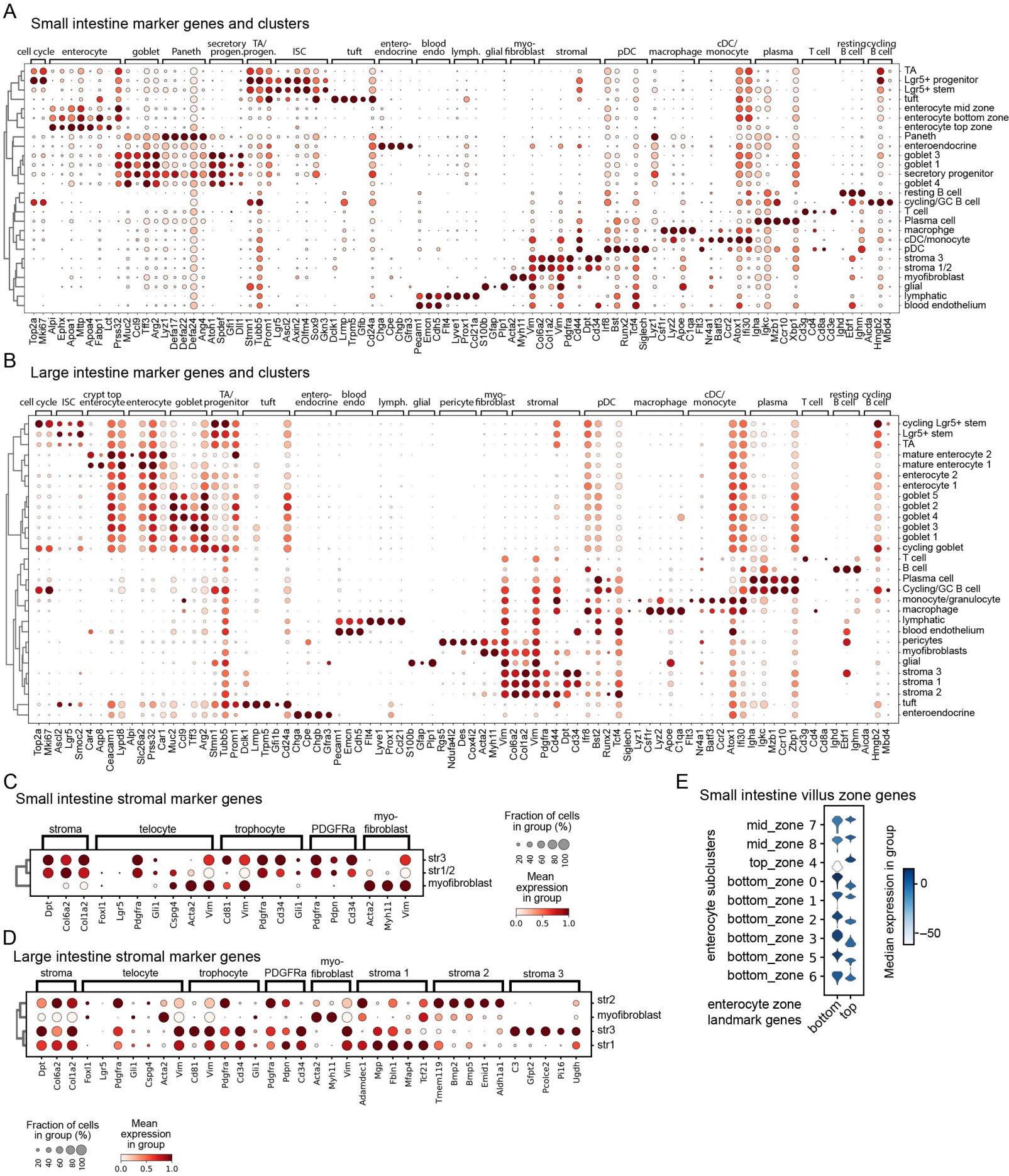

Figure S3. Dot plots show marker gene expression in each cluster of cells in the *in vivo* sequencing datasets, Related to Figure 4. (A-B) Expression of marker genes (excluding stromal cell clusters) in all clusters from the murine small **(A)** and large intestinal **(B)** scRNA-seq datasets. **(C-D)** Marker genes for stromal cells in the small **(C)** and large intestinal **(D)**. For all the plots in A-D: The size of the dots represents the fraction of cells with non-zero expression in each group, while the color indicates the log-transformed library size-normalized gene expression values. The final cluster IDs are listed at the bottom, genes are indicated on the left and their corresponding cell types are shown on the right. Lymph = lymphatics, pDC = plasmacytoid dendritic cell, cDC = classical dendritic cell, GC B cell = germinal center B cell, TA = transit-ampliflying cell. **(E)** Distribution of the expression of the mean z-scores of the top and bottom landmark genes reported by Moor et al. (2018) in each villus enterocyte subcluster of the small intestine dataset.

Supplemental Figure 4

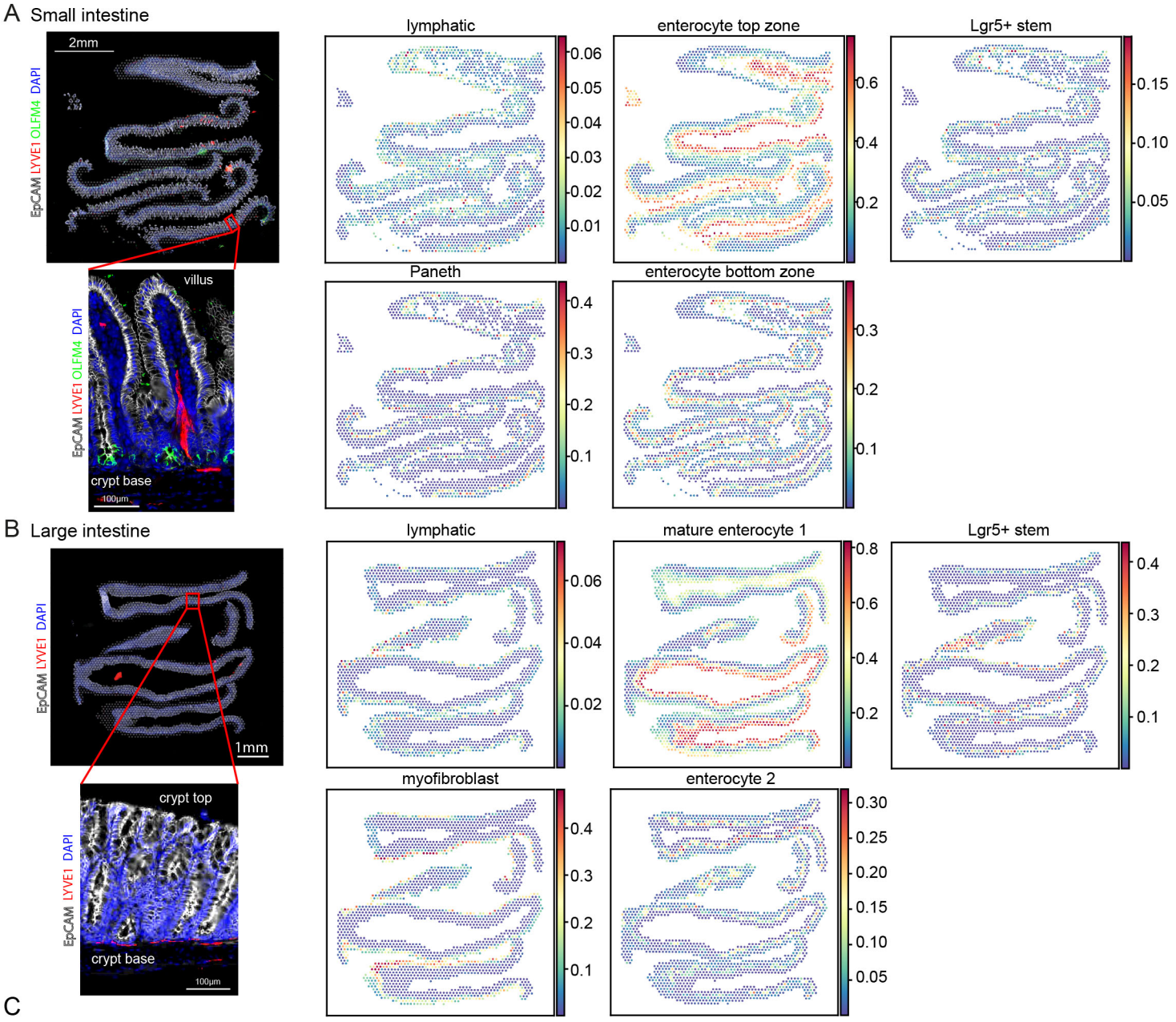

C

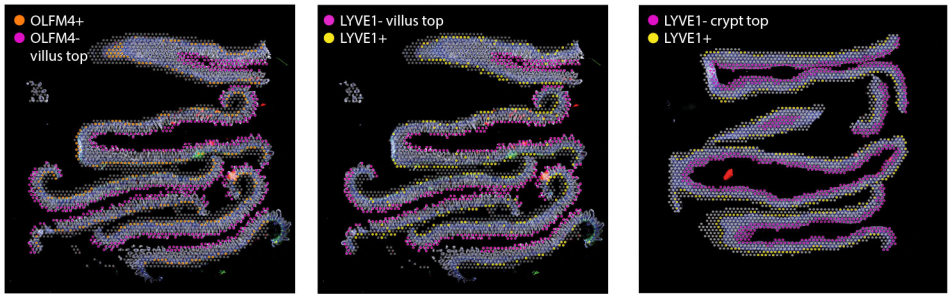

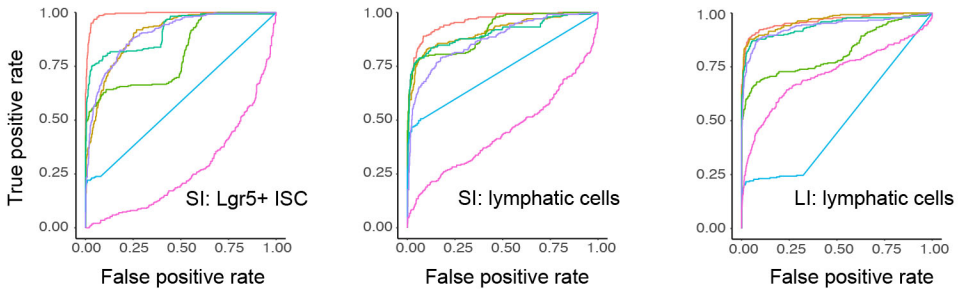

	SI: Lgr5 stem cells vs. OLFM4 IF	SI: Lymphatic cells vs. LYVE1 IF	LI: Lymphatic cells vs. LYVE1 IF
BayesPrism	0.992	0.958	0.964
Cell2location	0.902	0.910	0.963
destVI	0.809	0.912	0.818
RCTD	0.912	0.904	0.941
Stereoscope	0.900	0.873	0.937
Tangram	0.272	0.445	0.716
SPOTlight	0.588	0.730	0.497

method
- BayesPrism
- Cell2location
- destVI
- RCTD
- SPOTlight
- Stereoscope
- Tangram

Figure S4. **BayesPrism cell type deconvolution, Related to Figure 4. (A and B)** Immunofluorescence image of the mouse small intestinal (the top-left panel in A) and large intestinal (the top-left panel in B) tissue section used for spatial transcriptomic (10X Visium) profiling, each with higher magnification insets that were used in figure 4 below. $EPCAM^+$ epithelial cells are in white, $LYVE1^+$ lymphatics in red and $OLFM4^+$ small intestinal stem cells in green (OLFM4 is exclusive to small intestine). The overlaid gray dots on immunofluorescent images represent the 55 μm diameter RNA-capture areas. The rest of the panels show the fraction of indicated cell types with known spatial distributions inferred by BayesPrism (2^{nd} to 5^{th} panel in A and B). Color scales were clipped at the 99.5% quantile of each cell type for visualization. © Benchmarking inferred cell type fractions against immunofluorescence data as ground truth. Top row: ground truth of spots containing the cell types of interest (positive labels) was created by manually labeling spatial spots based on immunofluorescence of OLFM4 (for intestinal stem cells in the small intestine) and LYVE1 (for lymphatics in the small and large intestine). Negative labels were created by first excluding the positive labels followed by selecting spots from the top of villus, where no stem cell and lymphatics are expected. Bottom row: ROC curves (receiver operating characteristic curve) of each method. Table on the right shows the area of ROC curves for each method in each test data.

Supplemental Figure 5

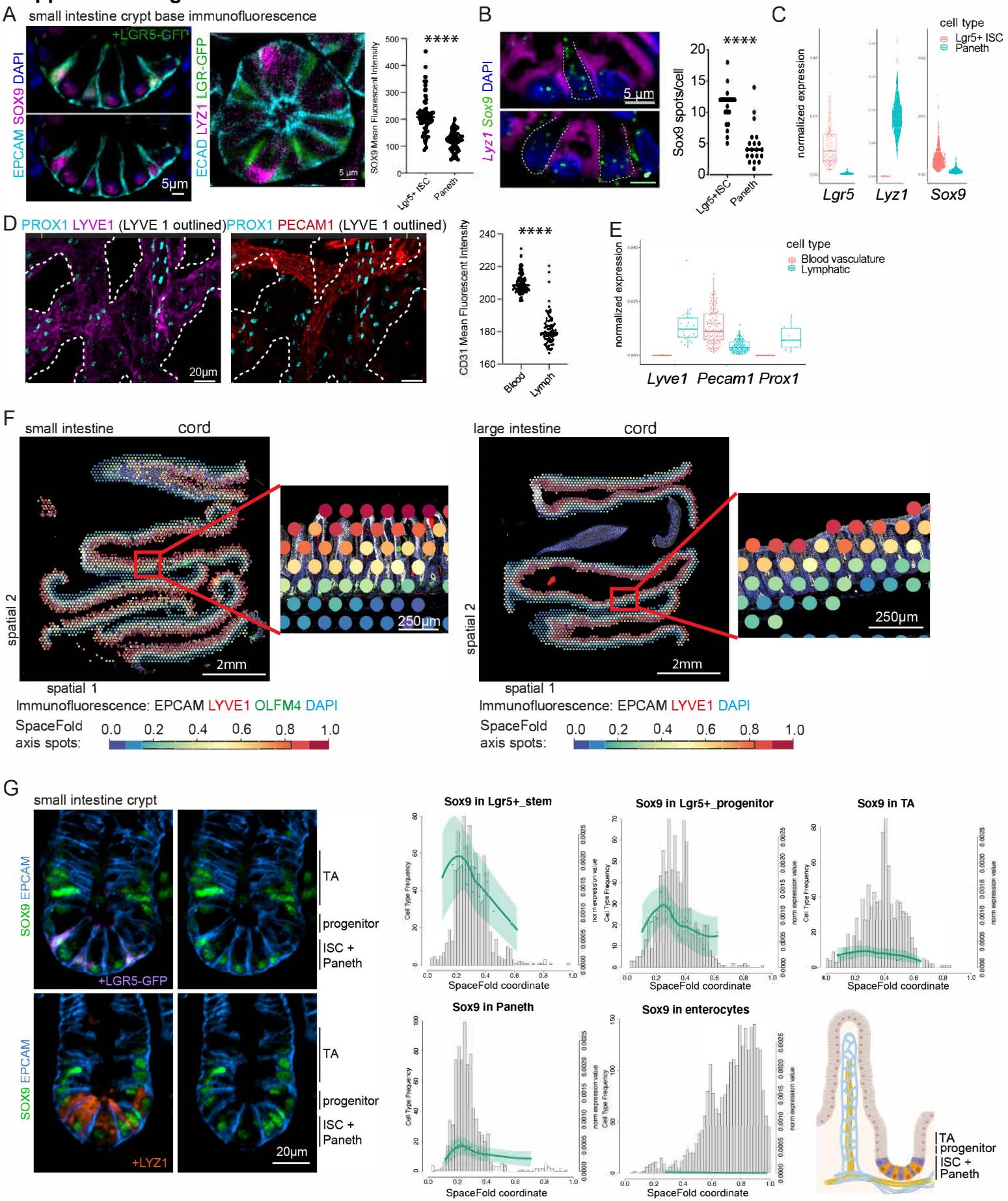

Figure S5. Validation of BayesPrism cell type-specific gene expression levels and SpaceFold spatial distribution of gene expression programs along the crypt-villus axis, Related to Figure 4 and Figure 5. (A) Immunofluorescent image of a small intestinal crypt base showing levels of SOX9 in adjacent LGR5-GFP+ EPCAM+ stem and LGR5-GFP- EPCAM+ Paneth cells. Right panel shows the fluorescence intensity of SOX9 in intestinal stem cells versus Paneth cells plotted as the mean fluorescence intensity/cell. **(B)** Representative image and quantification of *Sox9*+ spots in intestinal stem cells (*Lyz1*-) versus Paneth cells (*Lyz1*+) by fluorescence *in situ* hybridization (RNAscope). **(C)** Boxplots show normalized gene expression of *Lgr5*, *Lyz1* and *Sox9* in the intestinal stem cells and Paneth cells inferred by BayesPrism. Each dot represents one spatial spot containing the cell type of interest. **(D)** Immunofluorescence staining of PROX1 (aqua), LYVE1 (purple), and CD31/PECAM1 (red) with $LYVE1^{+}$ cells outlined to demonstrate low level expression of CD31/PECAM1 in LYVE1+ lymphatics, yet high expression in blood vessels ($CD31/PECAM1^{high}$) as quantified on the right. **(E)** Boxplots show normalized gene expression of *Lyve1*, *CD31/Pecam1* and *Prox1* in lymphatic and blood endothelial cells inferred by BayesPrism. Each dot represents one spatial spot containing both cell types of interest, while also having non-zero expression of the gene of interest. In C and E**,** Boxes mark the 25th percentile (bottom of box), median (central bar), and 75th percentile (top of box). Whiskers represent extreme values within 1.5-fold of the interquartile range. **(F)** Immunofluorescence images of the small and large intestinal 10X Visium tissue capture area overlayed with the pseudo-space axis projection by SpaceFold (as first presented in figure 5)**.** The red-boxed insets are magnified. The pseudo-space axis nicely recapitulates the physiologic parameters of the crypt-villus (small intestine) and crypt (large intestine) axes. **(G)** Left: Immunofluorescence images of mouse small intestinal crypts showing different levels of SOX9 (green) expression in LGR5+ stem cells (SOX9 high) and LGR5- Paneth (SOX9 low) and transit-amplifying (SOX9 low) cells at the top. The bottom panel shows SOX9 expression in LYZ1+ Paneth cells (orange) versus LYZ1- epithelial cells. EPCAM (blue) marks pan-epithelial cells and the localization of cell types is listed on the right and further clarified in the schematic on the far right. Right: SpaceFold maps cell type-specific expression of *Sox9* onto the small intestinal crypt-villus axis in indicated cell types. X-axes mark the relative SpaceFold

spatial coordinate. Histograms show the distribution of spots containing the selected cell types along the crypt-villus axis corresponding to Y-axes on the left. Y-axes on the right indicate the expression value. Each dot represents the mean expression over an interval of selected spots binned along the SpaceFold axis (x-axis). Lines mark the mean values fitted using local polynomial regression. Shaded areas represent the mean ± 2 standard error. For all experiments with asterisk, **** $p < 0.0001$ (Unpaired two-tailed Student's *t*-test).

Supplemental Figure 6

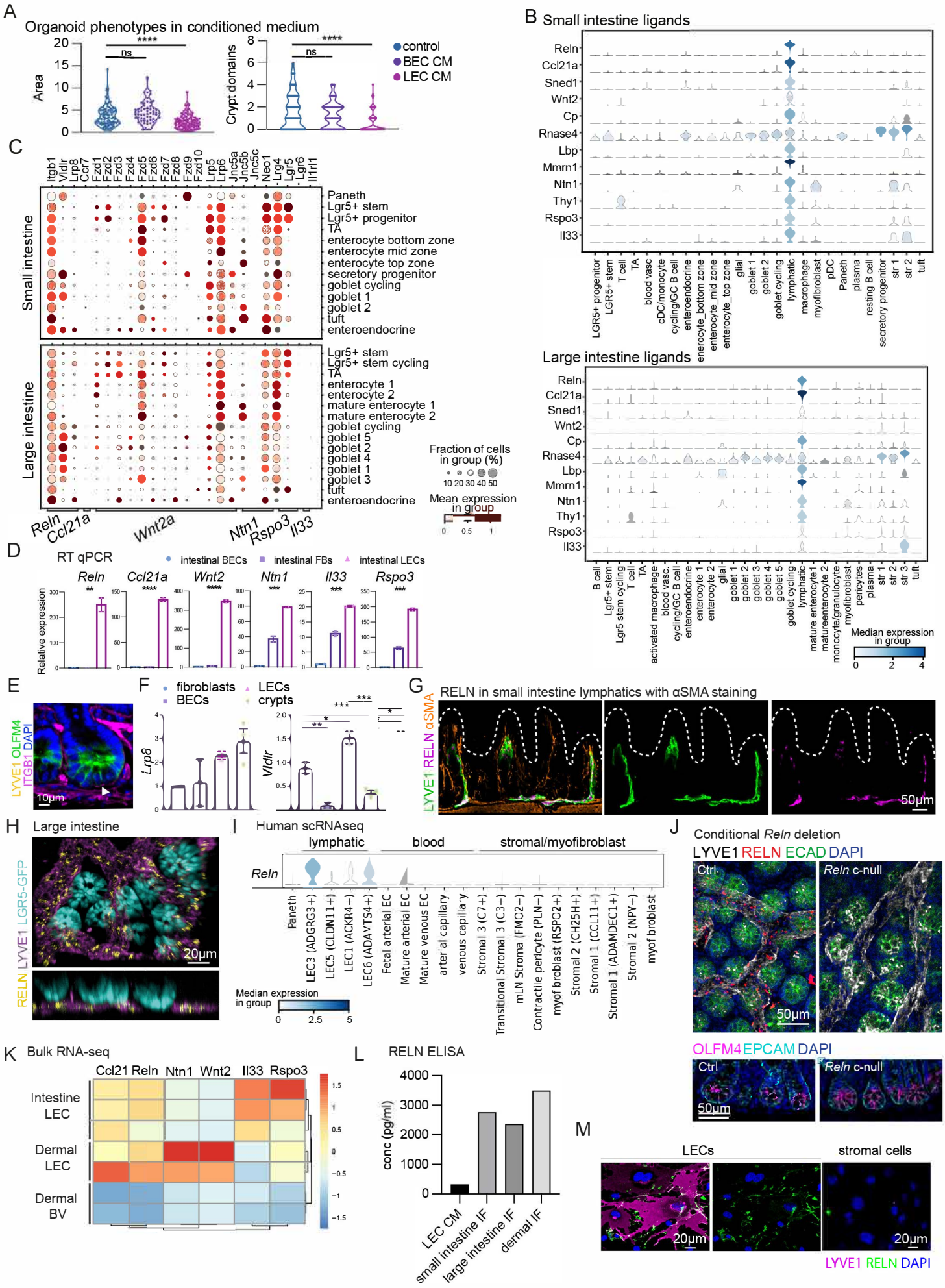

Figure S6. SpaceFold reveals a lymphatic signaling hub at the crypt base and exposes lymphatic-secreted factors that direct stem cell maintenance, Related to Figure 6. (A) Area and number of crypt domains per organoid of mouse small intestinal organoids grown in control medium versus BEC- or LEC-conditioned medium. **(B)** Distribution of log-normalized expression of candidate lymphangiocrine factors among small (top) and large (bottom) intestinal cell types (indicated at the bottom) computed using the scRNA-seq data shown in figure 4B and 4C, respectively. **(C)** Transcription level of putative receptors for selected lymphangiocrine factors (indicated at the bottom) among small (top panel) and large (bottom panel) intestinal cell types (indicated on the right) derived from small and large intestinal scRNA-seq datasets shown in figure 4B and 4C. Expression of ligand-specific receptors varies slightly between the small and large intestine, both of which express the most prominent receptors for each lymphangiocrine factor (e.g. *Itgb1*, *Vldlr* and *Lrp8* for Reelin). The size of dots represents the fraction of cells with non-zero expression in each group, while the color indicates the log-transformed library-size normalized gene expression values scaled between 0 and 1 for each gene. **(D)** Quantitative real-time PCR of selected lymphangiocrine candidates and their relative expression in intestinal BECs, fibroblasts (FBs) and LECs. **(E)** Representative immunofluorescent image showing the expression of active ITGB1 (pink) on the surface of OLFM4+ (green) stem cells in the murine small intestine. **(F)** Quantitative real-time PCR of two additional REELIN receptors, *Lrp8* and *Vldlr,* in small intestinal niche cell types (fibroblasts, blood endothelial cells (BECs) and lymphatic endothelial cells (LECs)) and crypts (epithelial + stem cells). **(G)** Immunofluorescence staining of REELIN (purple), LYVE1 (green) and alpha-smooth muscle actin (α-SMA, orange) in the distal small intestine; white outline is that of the villi determined by DAPI staining. **(H)** Whole-mount immunofluorescent image of mouse large intestinal tissue showing $LGR5^{+}$ stem cell-harboring crypts (cyan) sitting atop a network of $LYVE1^{+}$ lymphatic capillaries (purple), which express REELIN (yellow). **(I)** Log-normalized gene expression of REELIN in cell types of the healthy human small intestine as listed at the bottom (re-analyzed data from Elmentaite *et al*., 2021) **(J)** Whole-mount immunofluorescent staining of cleared small intestinal tissue from control (ctrl, $Reln^{fl/fl}$) and Reln conditional null (c-null, VE-Cad-CreERT2 $Reln^{fl/delta}$) mice showing maintained

lymphatic structure despite loss of REELIN in lymphatics. Representative of *n* = 2 mice/group. **(K)** Z-scored expression values of lymphatic-secreted factors from bulk RNA-sequencing of intestinal lymphatics and dermal lymphatics and blood vasculature (Gur-Cohen et al., 2019). Each row is an individual mouse. **(L)** Enzyme-linked immunosorbent assay (ELISA) for REELIN determining the levels of REELIN in LEC-conditioned medium, small intestinal, large intestinal and dermal interstitial fluid. Performed in duplicates. Concentration values (pg/ml) that were within range of the BSA standard curve are shown. **(M)** Immunofluorescence of REELIN (green) staining in cultured LYVE1+ (purple) lymphatic endothelial cells and stromal cells, which do not produce REELIN (negative control). For all experiments with asterisk, * p-value 0.01 to 0.05, ** p-value of 0.001 to 0.01, *** p-value of 0.0001 to 0.001, **** $p < 0.0001$ (Unpaired two-tailed Student's *t*-test).

Supplemental Table 1

Oligonucleotides (quantitative real-time PCR primers)		
Gene	**Forward sequence (5'-3')**	**Reverse sequence (5'-3')**
Lyz1	GAGACCGAAGCACCGACTATG	CGGTTTTGACATTGTGTTCGC
Muc2	CAAGTGATTGTGTTTCAGGCTC	TGGAGATGTTCTTGGTGCAG
Chga	CAGCAGCTCGTCCACTCTTT	GACGCACTTCATCACCTTGG
Alpi	CAGAACCTGGTGCAAACGTG	GTTGGCTCAAAGAGGCCCAT
Dclk1	CAGGAGTTTCTGTAATAGCAACCA	CCGAGTTCAATTCCGGTGGA
Lyve1	CAGCACACTAGCCTGGTGTTA	CGCCCATGATTCTGCATGTAGA
Flt4	CTGGCAAATGGTTACTCCATGA	ACAACCCGTGTGTCTTCACTG
Reln	GGACTAAGAATGCTTATTTCC	GGAAGTAGAATTCATCCATCAG
Ccl21a	AAGGCAGTGATGGAGGGGGT	CTTAGAGTGCTTCCGGGGTG
Wnt2a	CTCGGTGGAATCTGGCTCTG	CACATTGTCACACATCACCCT
Ntn1	CAGCCTGATCCTTGCTCGG	GCGGGTTATTGAGGTCGGTG
Il33	TGAGACTCCGTTCTGGCCTC	CTCTTCATGCTTGGTACCCGAT
Rspo3	ATGCACTTGCGACTGATTTCT	GCAGCCTTGACTGACATTAGGAT
Lrp8	GAATGAAGGCAGCCAGAT	GTTGTCGAAATTCATGCTC
Vldlr	GTGTACTTGAAGACCACTGAAGAG	GCTGGCTCTGTTACCATTC

Table S1. **Related to STAR methods.** Quantitative real-time PCR primer sequences used in this study.